Journal of Power Sources 218 (2012) 331–340

Contents lists available at SciVerse ScienceDirect

Journal of Power Sources

journal homepage: www.elsevier.com/locate/jpowsour

Bandwidth based electrical-analogue battery modeling for battery modules

Jianwei Li [a], Michael S. Mazzola [a,*], James Gafford [a], Bin Jia [b], Ming Xin [b]

[a] Center for Advanced Vehicular Systems, Mississippi State University, 200 Research Blvd., Starkville, MS 39759, USA
[b] Department of Aerospace Engineering, Mississippi State University, 330 Walker at Hardy Rd, Mississippi State, MS 39762, USA

HIGHLIGHTS

- Recognize the bandwidth characteristics of a commonly accepted battery model.
- Build model based on the bandwidth of the stimulus by assigning time constants.
- Model at the module level (vs. cell level), taking advantage of cell averaging.
- High fidelity has been proved for a Li-ion battery module on performance test.

ARTICLE INFO

Article history:
Received 9 May 2012
Received in revised form
27 June 2012
Accepted 1 July 2012
Available online 7 July 2012

Keywords:
Batteries
Parameter identification
Electrical model
Lithium-ion
State of charge
Bandwidth

ABSTRACT

A technique for building a high fidelity electrical-analogue battery model by identifying the model parameters at the module level, as opposed to the cell level, is proposed in this paper. The battery model, which is represented by electrical circuit components, can be easily integrated into popular simulation environments for system level design and predictive analysis. A novel bandwidth based time-domain procedure is introduced for identifying the model parameters by selective assignment of the limited bandwidth of the battery model approximation according to the natural bandwidth of the system that uses the battery. The aim of this paper is to provide an accurate off-line electrical-analogue battery model for simulation of larger systems containing large-format batteries, as opposed to a detailed electrochemical model suitable for simulation of internal battery processes. The proposed procedure has been experimentally verified on a 6.8 Ah Ultralife UBBL10 Li-ion battery module which is a "microcosm" for a modern large-format battery pack. A maximum 0.25% error was observed during a performance test with arbitrary but bandwidth-limited charging and discharging intervals characteristic of a typical battery application.

1. Introduction

Driven by the fast growing hybrid electric vehicle (HEV) and plug-in hybrid electric vehicle (PHEV) market, batteries are gaining greater attention because the battery pack is a key component [1,2]. High fidelity battery models that are applicable to high power and energy batteries and that are computationally tractable are needed by system designers, as they need a battery model which can be easily integrated into popular simulation environments for system level design and predictive analysis.

There are two main kinds of battery models available in the literature: physical models which are mainly electrochemical battery models, and behavior models, including mathematical models and electrical-analogue battery models. The term of "electrical-analogue battery model" was introduced, as opposed to "electrical battery model", to emphasize the fact that the model is actually an "analogue" of an electrical system rather than a model of specific electrical components (such as series internal resistance). In other words, the model is a state-space dynamical model represented by electrical components. The distinction is necessary because for the electrical-analogue battery models typically reported in the literature, the circuit components rarely represent the components of a real battery.

There are direct relationships between the battery electrochemistry and the parameters in the electrochemical models, which usually involve a number of coupled partial differential equations [3,4]. These models are complicated and comprehensive, which yield better accuracy than other types of battery models; but they are mostly used by battery designers for battery structure and material design. A disadvantage of the electrochemical models are

* Corresponding author. Tel.: +1 662 3255435; fax: +1 662 3255433.
E-mail addresses: lijwing@gmail.com (J. Li), lijwing@gmail.com, mazzola@ece.msstate.edu (M.S. Mazzola).

0378-7753/$ – see front matter © 2012 Elsevier B.V. All rights reserved.
http://dx.doi.org/10.1016/j.jpowsour.2012.07.006

that they are computationally intensive often making them too slow to execute for system level simulation [5–8]. For the behavioral models there are not necessarily direct correlations between the battery physical parameters and the model parameters. The scope of this work is to report on improvements in the procedures for estimating parameters of behavioral models. Modeling of detailed electrochemical processes internal to the battery is not treated in this work.

The mathematical battery models usually come from empirical or stochastic equations [9,10] drawn largely from static features of the battery terminal characteristics. These models are simple and fast in simulation, but when used in dynamic system simulation they are generally less accurate compared with other types of battery models [5,7]. In some circumstances they may be acceptable for low-power battery applications with slow dynamics, or where simulation accuracy is not strictly enforced. These models are not often used where batteries can be expected to experience strong dynamics, such as for the case of a battery pack in HEVs/PHEVs.

The electric circuit analogue battery model uses electric circuit elements such as voltage sources, current sources, resistors, capacitors and inductors to represent a real battery, although the procedure for identifying parameters and assigning them to the circuit elements often does not correlate with a specific equivalent physical element. In fact, the model is more accurately described as a truncated approximation of a non-linear system. The complexity of electrical-analogue battery models lies between the electrochemical models and the mathematical models [5,7]. Comparing the mathematical models and the electrical-analogue battery models, the mathematical models typically code equations curve fit to data that do not have the two-stage coupled form of the electrical-analogue battery model. The electrical-analogue model combines a separate estimator of the true open-circuit voltage (OCV) with state equations (RC networks) that model the dynamic series voltage obscuring the true OCV at the battery terminals. The former can be separately estimated using the state of charge (SOC)-OCV method described here. The fidelity of the latter can be improved as needed by increasing the order of the state equations (i.e., adding RC networks). Since these electrical-analogue models are represented by electrical circuit elements, they are inherently suitable for simulation software with circuit solvers for network analysis and thus are easily implemented into high-level power system design and simulation.

Various electrical-analogue battery models have been built and reported in the literature [5–8,11–18], however, the accuracy of most of the models are not acceptable for high fidelity system level modeling [11,14,18], or the procedure to extract the model parameters is challenging [8], or the modeling requires information about the physical parameters that may not be available to the general user [19]. The object of the modeling is usually a single battery cell instead of a battery assembly containing many battery cells, and more importantly is that much of the behavioral battery model research has taken the circuit components in the battery model as a representation of battery physical parameters, rather than as a behavioral representation of battery current-voltage (I–V) characteristics.

Since a real-world battery is a non-linear system [5,17,20], there should be no natural exponential moments if a finite number of exponential terms are used to approximate the battery behavior. The number of RC networks used in the electrical-analogue battery model is inherently limited and is equivalent to a truncated exponential representation of a non-linear system – a real-world battery. Thus when facing this inherent need to reconcile the practical limits of the approximation, preference should be given to the time constants of the exponential moments (RC networks in the battery model) that accommodate the desired battery stimulus or battery application. In other words, the time constants of the RC networks in the electrical-analogue battery model should be systematically chosen based on a specific battery stimulus or battery application bandwidth, rather than pursuing natural characteristics of the battery that may not be relevant to the system modeling objectives. Limiting the approximation to the relevant system-driven characteristics is the inherent reason for the improved accuracy reported here as verified by experimental observation.

In this paper, we examine constructing the dynamical representation of the electrical-analogue model based on the dynamical needs of the larger simulation. The temporal resolution of the larger simulation is constrained for many potential reasons. One will be the limitations of models other than the battery model. Another is temporal characteristics of the application. For example, an automobile powertrain will be operated within characteristic temporal limits that are natural to the application. A finite resolution battery model such as the one used in this paper can be “tuned” to this characteristic time scale. The procedures described in this paper are suitable for this process.

The proposed battery modeling aims at battery modules, especially large-format battery assemblies, and delivers high fidelity results. The advantage of this module level procedure is that non-idealities known to exist in battery modules consisting of many cells, such as weak cells, unbalanced cell state of charge and interconnection impedances, is captured self-consistently at the time the battery parameters are identified. In addition, module-to-module variation is less pronounced than cell-to-cell variation due to the cumulative effects of cell averaging. It is likely, then, that a battery model of the module will be more robust against such variation than a module model “built up” in a virtual sense by forming networks of an inherently idealized single cell model. To put it another way, to capture the same confidence in the terminal behavior of a large-format battery pack as gained by doing an actual experimental observation of the battery terminal characteristics it would be necessary to build statistical models of individual cells.

This paper identifies the electrical-analogue battery model parameters based on the bandwidth characteristics of the model with measurements of battery terminal voltage and current. The open-circuit voltage versus state of charge profile is initially estimated with a rapid test method [20], and then improved based on a test profile designed for the purpose. The proposed parameter identification technique is experimentally verified on a 6.8 Ah Ultralife UBBL10 Li-ion battery with a maximum error of 0.25%.

This paper is organized as follows. Section 2 describes the electrical-analogue battery model. Section 3 presents the parameter identification algorithm for the electrical-analogue battery model. Section 4 details the procedure to extract the SOC–OCV profile. Section 5 explains the experimental test apparatus. Section 6 discusses the verification of the battery model. Section 7 concludes this paper.

2. The electrical-analogue battery model

A well-recognized electrical-analogue battery model of Lithium-ion batteries [5,7,8,16,17] is shown in Fig. 1. It includes two parts: the left part is the state of charge estimator, which estimates battery SOC based on coulomb-counting as shown in Eq. (1) (DOD: depth of discharge); the right part is an electrical network that is a circuit representation of a truncated approximation of the dynamic response of the electrochemical battery system. A circuit representation is easily integrated into circuit simulation software for self-consistent electrical analysis within a larger system simulation. The bridge between these two parts is the SOC–OCV

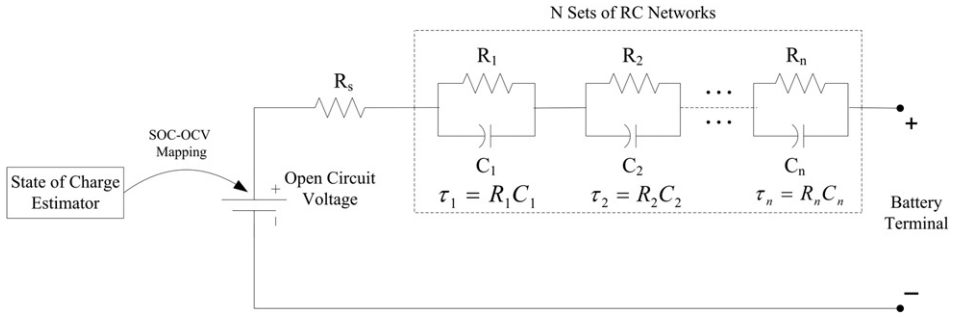

Fig. 1. The electrical-analogue battery model: the left part is the SOC estimator; the right part is an electrical network that is a circuit approximation of the dynamic response of the electrochemical battery system.

mapping which represents the unique functional relationship between battery state of charge and internal voltage potential, where the internal voltage potential is often referred to as battery open-circuit voltage (OCV) measured at the battery terminal after 24 h relaxation [20].

$$\mathrm{SOC} = \mathrm{SOC}(0) - \frac{\int_0^{t_f} i(t)\mathrm{d}t}{C}; \quad (\mathrm{DOD} = 1 - \mathrm{SOC}) \tag{1}$$

In the battery model, the battery terminal voltage is a reflection of the battery open-circuit voltage, internal resistance, and transient effects caused by charging or discharging current. By measuring battery terminal current, the SOC can be estimated from (1) if the initial SOC is known. If the initial SOC is not known but the battery has been left at rest for a long time (more than 24 h), the initial SOC can be estimated from the SOC–OCV mapping in a reverse direction by measuring the initial battery terminal voltage [20]. Otherwise recursive estimation algorithms can be used to get an initial estimate of the SOC [21–23]. Once the battery SOC is known, the battery open-circuit voltage can be found from the SOC–OCV mapping. In (1), the battery capacity C value will change as the battery ages and with temperature as well, but since this time variance is very slow compared to the electrical dynamics required for the system application, the authors have assigned a constant value. While battery aging is not explicitly addressed in this paper, such latent time variance could be included in future work.

The entire model is dynamical, but different components approximate different features of the dynamic response of a real battery. For example, the series resistance R_s captures changes in the battery potential that are faster than explicitly modeled by continuous state variables. The N sets of RC networks are employed to model with continuous state variables, having time constants $\tau_1, \tau_2, \ldots, \tau_n$, themselves a limited fraction of the dynamic response of the electrochemical processes caused by charging or discharging currents. One interpretation, used in this work, is that the RC network is a truncated exponential representation of a non-linear system, which is a common engineering problem [24,25]. Although electric circuit components are used in this model, the model does not directly represent battery physics or chemistry, but instead is a dynamical approximation of the battery behavior observable at the battery terminals.

Since there are several time constants $\tau_1, \tau_2, \ldots, \tau_n$ in the model, which are directly related to the dynamic responses and thus comprise the key components of the model, then the bandwidth of the battery model is approximately limited to $[1/\tau_{max}, 1/\tau_{min}]$. The battery model therefore can approximate continuous dynamics only within the design bandwidth. Dynamics outside of this bandwidth are only asymptotically represented. For example, dynamics that are significantly faster than τ_{min} are modeled as discontinuous voltage variations, the magnitude of which is computed as the product of the series resistor R_s in Fig. 1 and the change in the terminal current between time steps. Conversely, dynamics slower than τ_{max} are represented only by the change in OCV that follows the state of charge integrator expressed in Eq. (1). This description of the electrical-analogue battery model as essentially a mathematical approximation designed as an optimal curve fit to a dynamic system, rather than an attempt to assign physical meaning to the model components, is a novel approach with respect to the literature. It opens the possibility of recognizing that the model is used as part of a larger simulation, and the simulation's objectives, characteristics, and limitations can be more important than the fidelity of any one model itself. Indeed, it is common to over specify the fidelity of models without considering the context of the simulation.

This model was originally developed in [5] and it was verified on low-power battery cells in portable electronics. A modified parameter identification algorithm based on the bandwidth limitation characteristic of the model is developed in this paper, together with an improved SOC–OCV extraction method. Another improvement over the original work is that the proposed modeling procedure aims at modeling a battery module as a whole instead of a single cell. In this case the cell balancing, cell discrepancy and scaling issues are already included and solved in the modeling process. Thus the module-based battery model is readily integrated into larger systems for system level design and simulation, e.g., selecting the most appropriate battery modules for a power electronics system.

Battery models can be used in two ways: on-line and off-line. An on-line battery model is used when instantaneous measurements of battery current and terminal voltage are fed into the model to estimate the internal state variables – most importantly, the battery state of charge. Accurate estimation of SOC and other parameters can be achieved by using state-estimation filter technology [13,22,26]. These kinds of battery models are applicable to battery management systems. The emphasis of these models is the filter included in the model, but not the model itself, although the final performance of the filter does rely to some extent on the quality of the battery model. On the other hand, an off-line battery model is used without new environmental inputs, focusing on predicting battery behavior such as terminal voltage and SOC based on past and current battery state and stimulus from the external circuit. The accuracy of these models greatly depends on carefully identified model parameters. These kinds of models are mostly used for system level design, such as evaluating for the most appropriate battery modules in simulation before physically building a larger system. While both types of applications can be

addressed successfully with the method reported here, the application of interest in this paper is the off-line one.

3. Parameter identification

3.1. The workflow

Since the bandwidth of the electrical-analogue battery model is limited, the battery model should be applicable to the bandwidth requirements of a particular application environment. In other words, for system level simulation, the battery model should be responsive to the dynamic stimulus of the system, rather than designed in a component centered procedure. Given the possibility that the same battery may exhibit a different dynamic response in different systems (primarily due to the non-linearity of the battery and the finite bandwidth of the system), then the difference should be accommodated in the parameter identification procedure. Fig. 2 illustrates the proposed workflow. It starts by analyzing the battery application environment, i.e., the designed battery operation bandwidth. Then the bandwidth of the model should be determined based on the application. Battery tests are to be designed according to the desired bandwidth of the model. Finally, mathematical tools such as the non-linear least squares algorithm are used to identify the model parameters. Hence an application-oriented battery model can be achieved.

3.2. Battery application environment and the bandwidth of the model

The battery modeling process starts from analyzing the bandwidth of the desired battery application environment. Once the application bandwidth $[f_{min}, f_{max}]$ is estimated, the time constants of the RC works in the model should be designed to accommodate the application bandwidth. Particularly, at least two time constants τ_{min} and τ_{max} need to be formed as $\tau_{min} \approx 1/f_{max}$ and $\tau_{max} \approx 1/f_{min}$. More RC networks can be added to the model with time constants in between τ_{min} and τ_{max} to add to the model's fidelity.

3.3. Design battery tests

Behavior battery tests were designed for this research similar to [20] and with several different current rates. Fig. 3 shows the behavior test profile with 0.4 C current where 1 C current is the current that will discharge a battery from 100% SOC to 0% SOC in 1 h. The battery module was charged to full SOC and then left to rest for more than 24 h before the behavior test. A pulse discharging/charging cycle was used in the behavior test for two reasons: (1) to extract the circuit components parameters; and (2) to get an initial estimate of the SOC–OCV profile. The length of the discharging/charging pulse was chosen to modulate the battery SOC by about 10%. Each pulse was followed by a 1 min rest to observe the dynamic response of the battery when there was no current. Between the discharging test and the charging test, the battery module was allowed to rest for 24 h to let the battery reach steady state. The behavior tests were conducted over 10–100% SOC for safety reasons, which embraced the normal operating range of a battery module in automotive and other power applications. The power supply is capable of both constant current charging and constant voltage charging. When the voltage set point was met during constant current charging, the charging mode changed to constant voltage charging automatically. The charging/discharging pulses were controlled manually based on the charging/discharging time interval.

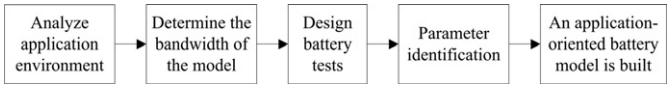

Fig. 2. The proposed workflow of the application-oriented battery modeling.

3.4. Identify model parameters

3.4.1. Mathematical description of the electrical-analogue battery model

A two RC network representation of the battery model is the current level of approximation found in similar advanced work and is thus also selected for this work as illustrated in Fig. 4.

Taking capacitor voltages V_{c1}, V_{c2} and battery SOC as three state variables, the mathematical representation of Fig. 4 is derived as Eqs. (2) and (3) based on circuit laws and Eq. (1). The positive current is taken as when battery is being charged. Terminal current i_t and terminal voltage V_t are the two quantities that can be directly measured at the battery terminals. The parameters which need to be identified are R_s, R_1, C_1, R_2, C_2, while battery capacity C in Eq. (2) is assumed to be constant. Battery open-circuit voltage V_{ocv} is an eighth-order polynomial equation in SOC, which is discussed in Section 4.

$$\begin{bmatrix} \dot{V}_{c1} \\ \dot{V}_{c2} \\ \dot{\mathrm{SOC}} \end{bmatrix} = \begin{bmatrix} -\frac{1}{R_1C_1} & 0 & 0 \\ 0 & -\frac{1}{R_2C_2} & 0 \\ 0 & 0 & 0 \end{bmatrix} \begin{bmatrix} V_{c1} \\ V_{c2} \\ \mathrm{SOC} \end{bmatrix} + \begin{bmatrix} \frac{1}{C_1} \\ \frac{1}{C_2} \\ \frac{1}{C} \end{bmatrix} i_t \tag{2}$$

$$V_t = V_{ocv}(\mathrm{SOC}) + R_s i_t + V_{c1} + V_{c2} \tag{3}$$

3.4.2. Identifying the parameters

From Eqs. (2) and (3), the parameters that need to be identified are R_s, R_1, C_1, R_2, C_2. C is a constant representing battery capacity. Although there are five parameters to be identified, there are only three degrees of freedom because the products R_1C_1 and R_2C_2, which are the two time constants of the RC networks, are predetermined and kept constant.

To identify the parameters, the error between the estimated terminal voltage V_{t_est} and the measured terminal voltage V_{t_mea} is calculated each iteration. Then the objective function Q to be minimized is formed as Eq. (4), where k is the index of the samples.

$$Q = \sum_{1}^{k} \mathrm{err}(k) = \sum_{1}^{k} (V_{t\_mea}(k) - V_{t\_est}(k)) \tag{4}$$

The non-linear least-squares (NLS) algorithm is used to minimize Q in each rate window.

The rate window for parameter identification is chosen as one complete pulse charge or discharge period plus the associated following rest period. As illustrated in Fig. 5, the rate window can be divided into five parts: (1) instantaneous voltage drop after discharging current is applied to the battery, which is reflected by the voltage change on R_s; (2) transient period dominated by τ_1 and τ_2; (3) transient period dominated by τ_2 ($\tau_2 > \tau_1$), because the state variable associated with τ_1 vanishes after a short period; (4) instantaneous voltage rise after discharging current is turned off, which is reflected by the voltage change on R_s; (5) transient period dominated by τ_1 and τ_2 during the rest period. Although we recognize the effects of each circuit parameter on approximating battery dynamic responses, all the data points in each rate window

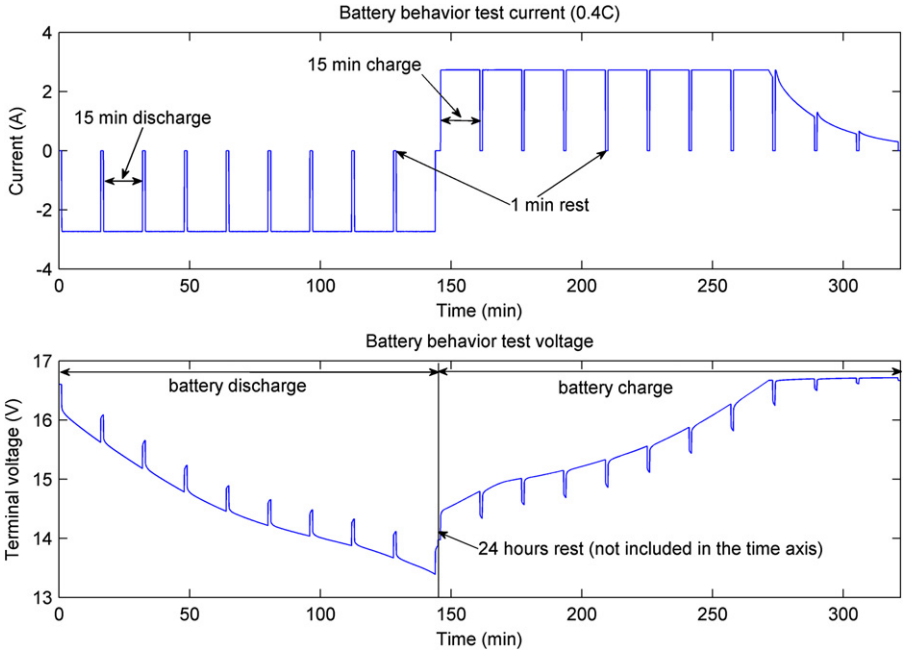

Fig. 3. Battery behavior test with 0.4 C current (1 C current is the current that will discharge a battery from 100% SOC to 0% SOC in 1 h).

are taken as a whole while using NLS. When multiple rate windows exist in the battery test, the identified parameters from NLS change with rate windows (see Fig. 6).

3.4.3. Choosing single set of the parameters

Fig. 6 shows the identified parameters using the NLS algorithm with three current rates: 0.4 C, 0.3 C and 0.2 C. In this figure, the identified parameters change with SOC and current rate, an observation reported in the literature by others [5,15,16]. However, the change of the identified parameters does not necessarily reflect the optimal selection of the parameters, but rather an ensemble of local minimums of the objective function for different rate window and current rate. Thus a range of the parameters can represent the circuit parameters to some degree of approximation. This assumption is examined in Figs. 7 and 8.

Fig. 7 compares all the transient responses from three behavior discharging tests. From this figure we can see that the transient responses behave very similar to each other regardless of the SOC and current rate. And also the voltage is almost proportional with current rate. Note that the starting points of all the transient responses do not coincide at the same point for comparison, because the measured data depend on a sampling process which is not synchronized with the battery current modulator. This made it impossible to know the exact starting time of the transient period. Fig. 8 shows the manually calculated R_s from all behavior tests. Since the resistor R_s is responsible for the instantaneous voltage change, the value of R_s can be calculated directly with Ohm's law from the test data. The mean value of R_s is 0.1383 Ω with a standard distribution of 0.0034. Since the calculation of R_s also depends on the sampling frequency, different R_s values can be calculated at different sampling frequencies, or the same sampling frequency but a different sampling instant. Thus calculating R_s from individual cycles is of limited value and should not be used directly, however, the mean value of R_s can still approximately represent an effective estimate for this parameter under the sampling frequency used in the test. This observation highlights the true role of R_s, which is to capture the change due to un-modeled state variables with dynamics having a shorter duration than the sampling period of the experiment. One consequence of considering the influence of the

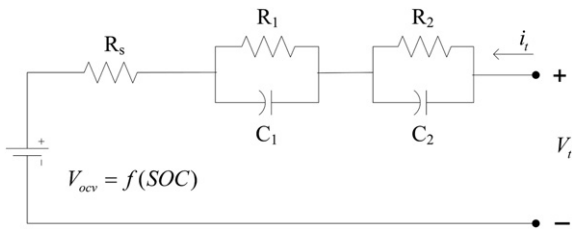

Fig. 4. Two RC network representation of the battery model.

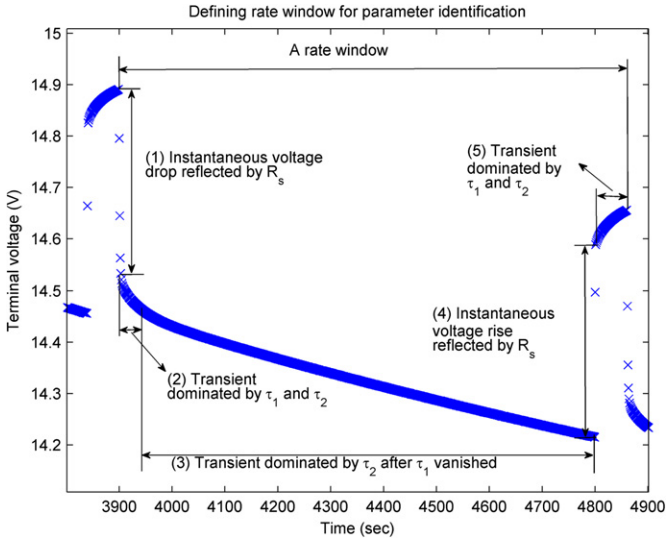

Fig. 5. Defining rate window for parameter identification: the rate window is chosen as one complete pulse charge or discharge period plus the associated following rest period.

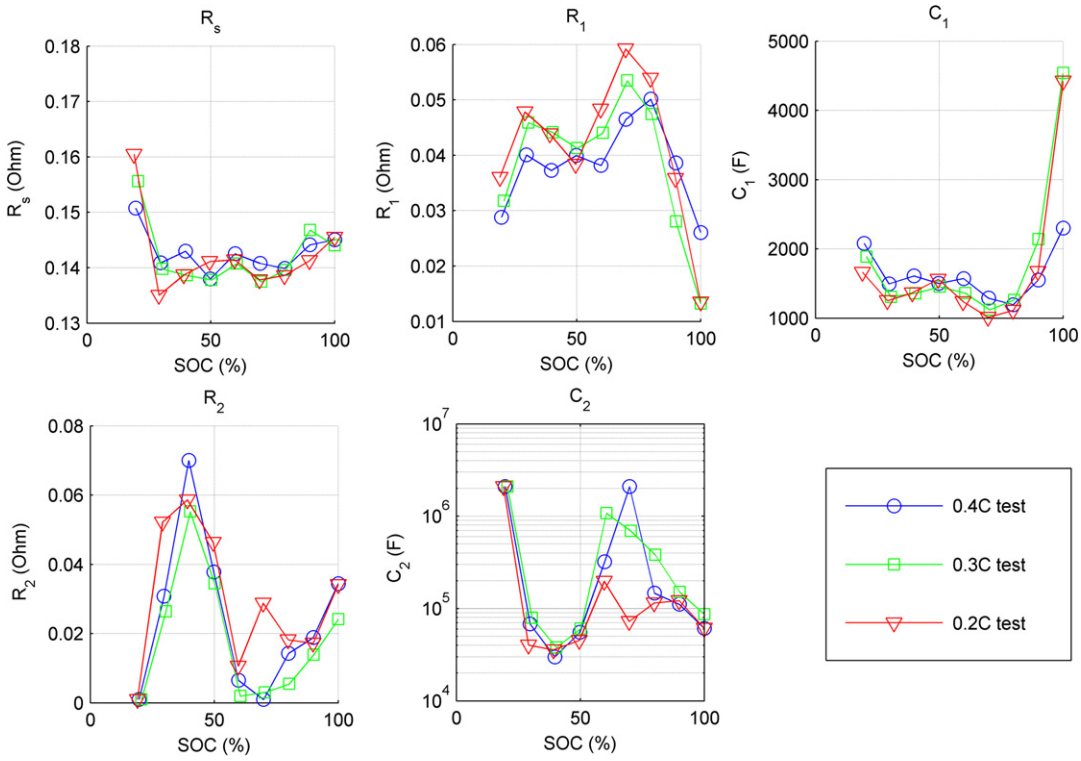

Fig. 6. Identified circuit parameters for a 6.8 Ah Ultralife UBBL10 Li-ion battery module.

discrete sampling time on the experimental observation of dynamic behavior during the construction of the dynamic model is that assigning a static "DC resistance" meaning to R_s is recognized as counter-productive to the fidelity of the dynamic simulation.

We suggest one process here, among a number of possibilities, for selecting a set of parameters from the ensemble of identified parameters. Since during normal operation, the battery module is usually operated around a particular SOC, a set of parameters near that SOC can be reasonably assumed to work best for the battery model. Then some manual curve fitting within a narrow range can be done based on the chosen set of parameters to achieve better overall performance among all rate windows while sacrificing some fitting accuracy in the rate window around the characteristic operating point. This step finalizes the building of the electrical-analogue battery model.

4. The extraction of the SOC–OCV profile

Accurate SOC–OCV profiling is a key factor for achieving a high fidelity electrical-analogue battery model. A two-step process has been established to make the best estimate of the SOC–OCV profile in a reasonable amount of time. The traditional way of obtaining the battery SOC–OCV profile is inefficient and time-consuming, because the battery transients must be allowed to vanish after

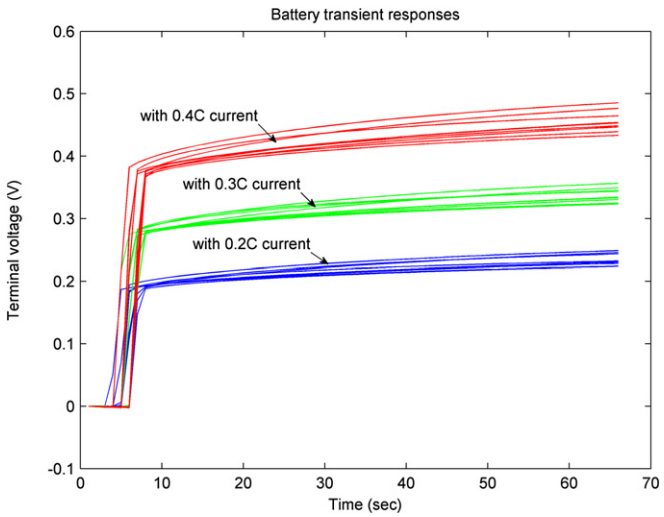

Fig. 7. Battery transient responses from three behavior discharging tests.

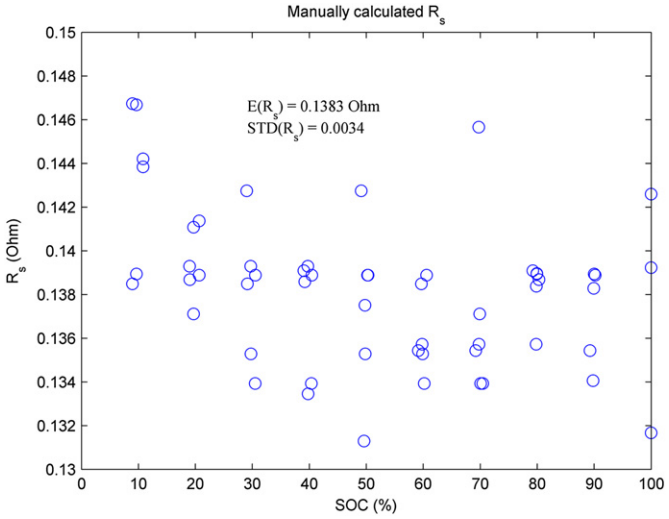

Fig. 8. Manually calculated R_s from all charging and discharging behavior tests.

a long period, typically cited as 24 h [20]. To get multiple points on the SOC–OCV profile, several weeks are needed to complete the test. A rapid test procedure is known to accelerate the process [20], however, as pointed out in [20], the accuracy of the extracted SOC–OCV profile needs to be improved to meet the demand for higher fidelity modeling.

The proposed algorithm for extracting the SOC–OCV profile includes two steps: the rapid test procedure to get an initial estimate of the battery SOC–OCV profile, and then four points on the SOC–OCV profile were measured after longer rest periods to make refinement to the profile toward the true OCV. This algorithm was experimentally verified on a 6.8 Ah Ultralife UBBL10 Li-ion battery module, as discussed next. The number of points for refining depends on the fidelity requirement of the model. For example, the four refining points performed in this work resulted in halving the total mean error as discussed in Section 6. However, the more refining points that are taken, the longer the test time will be. Quantitatively, adding a single refining point will increase the test time by 48 h, as each refining point requires one discharging rest period (24 h) and one charging rest period (24 h).

Fig. 9 shows the initial extraction of the SOC–OCV profile based on a complete discharging/charging cycle at 0.4 C rate (the behavior test shown in Fig. 3). The ending points of the rest periods from the charging test are connected by the green dotted lines, and the ending points of the rest periods from the discharging test are connected by the blue dotted lines. An average of the green line and the blue line is computed and drawn as the red line. Similar profiles are extracted from the other two behavior tests (at 0.3 C rate and 0.2 C rate). Minor differences are observed between these profiles so an average of the three red lines is used as the initial extraction of the SOC–OCV profile.

The second step is an improvement over the method in [20]. After the initial SOC–OCV extraction, the profile is further refined with another pulse discharging/charging cycle that contains several long rest periods of 24 h. In the behavior tests, the rest period is limited to 1 minute. By letting the battery rest for 24 h, we can observe a truer estimate of the battery open-circuit voltage by measuring the battery terminal voltage, as it is assumed that the battery transients have vanished after 24 h.

Fig. 10 shows the refinement of the SOC–OCV profile based on a new test profile with longer rest periods. Four points were chosen to refine the SOC–OCV profile at about 25%, 50%, 75% and 100% of SOC. The battery module was allowed to rest for 24 h after each pulse discharging/charging. This test started with battery discharging after the battery was charged fully and left for 37 h; and ended with charging back to full state of charge. The same criteria defining a fully charged battery was used before the test and at the end of the test, however, the final SOC went beyond 100% by 1% based on the coulomb-counting method, primarily because the battery was not fully reversible, especially in the high SOC range, which introduced small systematic error in calculating the SOC with the coulomb-counting method.

If the initial estimate of the OCV profile is correct, the battery terminal voltage should reach it after the long rest period, which would mean reaching the red line in Fig. 10. As observed from Fig. 10 the ending points of the rest periods fail to lie exactly on the red line, thus the SOC–OCV profile extracted from the three behavior tests should be corrected accordingly with linearly spaced vectors between two successive refining points, which is represented as the black curve. The point at about 14% SOC is not used to refine the SOC–OCV profile because the rest periods at that point are only two minutes altogether. Continuing the same procedure will refine the SOC–OCV profile at lower SOC range, but that was not done in this work.

5. Test apparatus

The test apparatus used for the battery tests is shown in Fig. 11, including a power source, a current sink, a shunt, a data logger, and a computer connected to the data logger. On the left is the UBBL10 Li-ion battery module. The power source is a Tenma 72-6905 DC Power Supply (maximum voltage = 30 V; maximum current = 3 A). The current sink is a Computerized Battery Analyzer CBA 2 from West Mountain Radio, which is a pure resistance power dissipater with a maximum power of 100 W. The shunt is a calibrated 5-mΩ resistor rated for 10 A. The current is calculated from the shunt voltage divided by the shunt resistance; the battery voltage is measured from the battery terminals. Two temperature sensors located on the front and rear surface of the battery measure battery case temperature. A third temperature sensor is used to measure the ambient temperature. Large-diameter, short wires are used in the apparatus to achieve minimum voltage drop on the wires. Two

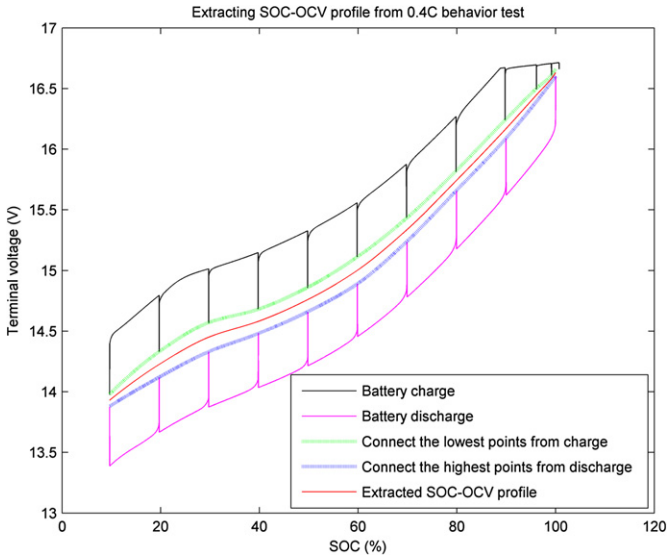

Fig. 9. Initial extraction of the SOC–OCV profile.

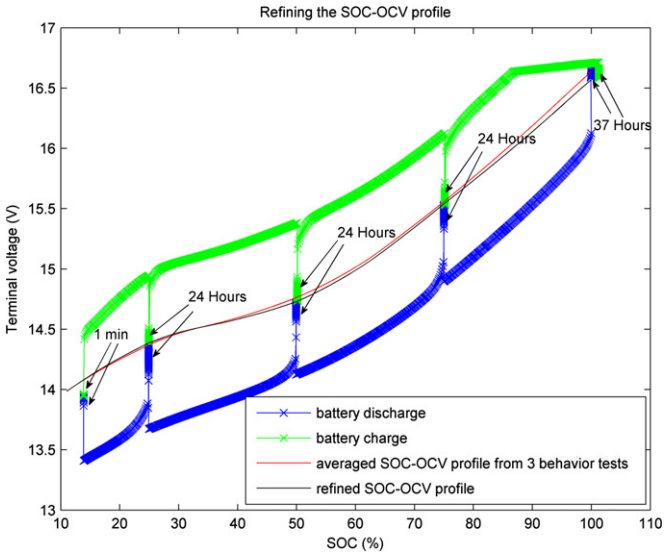

Fig. 10. Refining the extracted SOC–OCV profile based on a new test profile with longer rest periods. Four points were chosen to refine the SOC–OCV profile at about 25%, 50%, 75% and 100% of SOC.

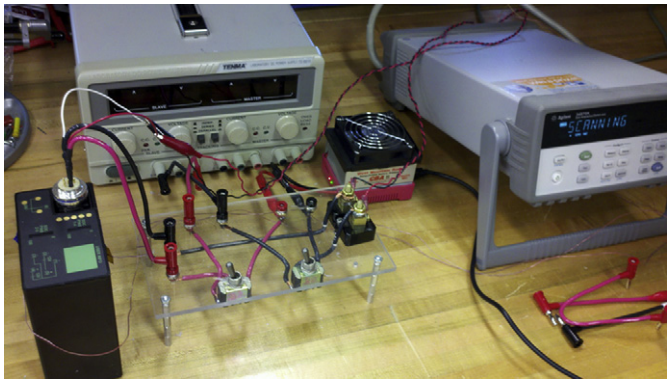

Fig. 11. Test apparatus.

switches are placed in the panel to switch the battery terminal between the power source and the current sink.

6. Model verification

The proposed battery modeling procedure was experimentally verified on a 6.8 Ah Ultralife UBBL10 Lithium-ion battery module as shown in Fig. 11. There are two battery assemblies, or sections, in the module, which can be connected in series or parallel. One section is selected in the test for model verification. Since a real battery module is a non-linear system [5,17,20], an arbitrary number of exponential moments can be used to approximate it, depending on the fidelity requirements. In this work we use two RC networks in the model as shown in Fig. 4.

The battery SOC–OCV profile was extracted according to the detailed process in Section 4. The OCV refining process is critical to the overall model accuracy, as when four OCV points were chosen for refining, the model mean error over performance test was halved compared with the one without OCV refining.

Because the rest time for the behavior tests is 1 min and the discharging/charging pulse lengths are 15 min (0.4 C), 20 min (0.3 C) and 30 min (0.2 C), one time constant at $\tau_1 = 60$ s and one at $\tau_2 = 2100$ s are employed to embrace all the transient periods in the behavior tests, assuming the battery behavior tests were designed for a certain battery application with this characteristic bandwidth. Please note that in this example these two time constants are predetermined before identifying the circuit parameters but after the behavior tests were conducted. But if the bandwidth of the battery application is known, the time constants should be chosen first, and then behavior tests should be designed according to the desired bandwidth of the battery application. In other words, since the electrical-analogue battery model is application-oriented, the time constants in the battery model should be chosen based on application, and accordingly the behavior tests designed to stimulate the actual battery should be within this bandwidth.

Three sets of behavior battery tests were conducted in the lab with 0.2 C, 0.3 C and 0.4 C current. The identified parameters are plotted in Fig. 6. As discussed in Section 3.4.3, a single set of parameters near 50% SOC of the 0.4 C test was selected to initialize the battery model as shown in Table 1.

After the parameters were initially identified, a behavior test with different current rates was conducted to manually refine the identified parameters to achieve better terminal voltage fitting (an automated process has been developed for this step that will be reported in a future publication). Fig. 12 shows the behavior test current profile. By adjusting the circuit parameters to better fit the estimated terminal voltage to the measured terminal voltage, the parameters are adjusted to those shown in Table 2. Fig. 13 shows the terminal voltage curve fitting results with a Mean Square Error (MSE) of 2.7674×10^{-4} V^2.

The performance battery test was designed and conducted in the lab to verify the battery model with parameters shown in Table 2. The test current and battery SOC are shown in Fig. 14. The

Table 1
Initially identified parameters.

R_s (Ohm)	R_1 (Ohm)	C_1 (kF)	R_2 (Ohm)	C_2 (kF)
0.1380	0.0400	1.5000	0.0378	55.5110

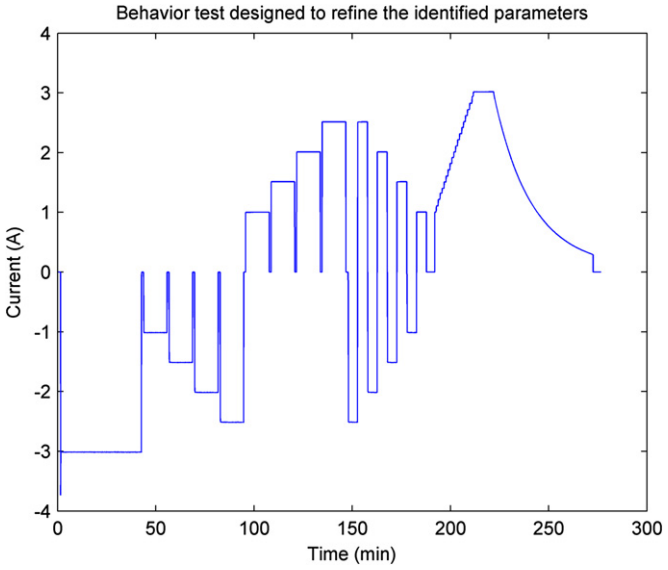

Fig. 12. Behavior test for manually refining the parameters.

Table 2
Manually refined parameters.

R_s (Ohm)	R_1 (Ohm)	C_1 (kF)	R_2 (Ohm)	C_2 (kF)
0.1383	0.0400	1.5000	0.0440	47.7270

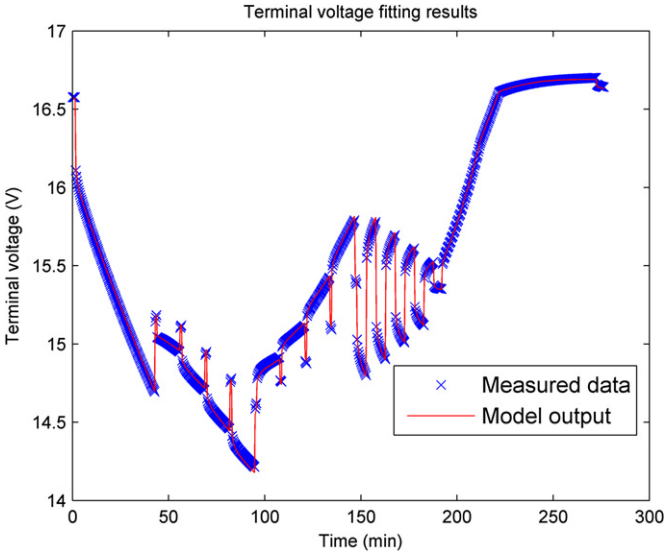

Fig. 13. Terminal voltage fitting results based on the refined parameters.

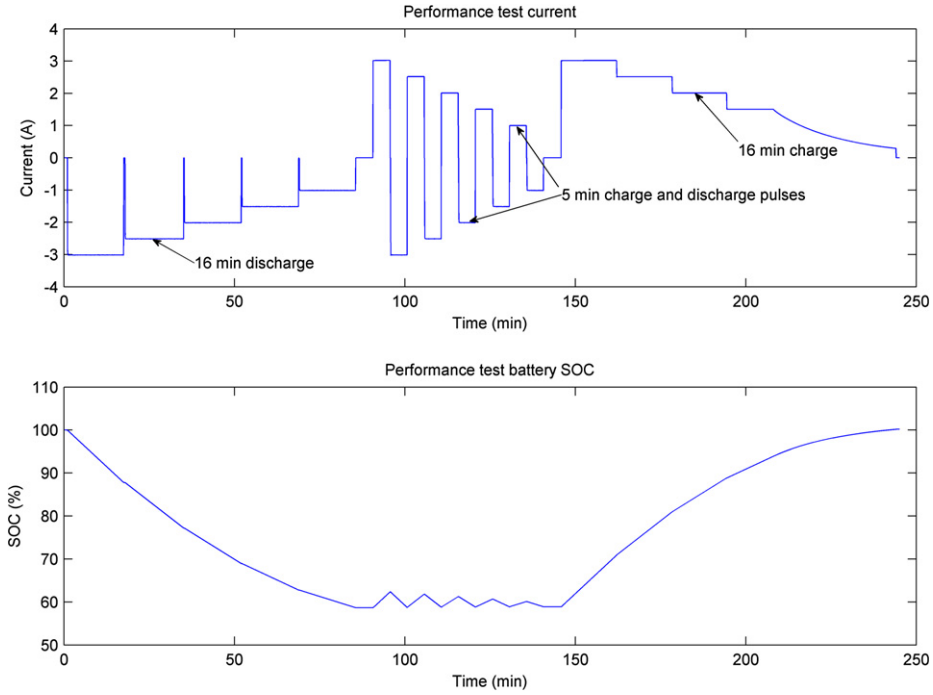

Fig. 14. Battery performance test profile.

battery module was firstly discharged to about 60% SOC from full SOC with five discharging current rates: 3 A, 2.5 A, 2 A, 1.5 A, and 1 A. Each of the current rates was applied in turn for 16 min. Then pulse discharge and pulse charge were conducted in turn with each of the five current rates. The interval of each current rate was 5 min. Finally, the battery module was charged back to full SOC with a variety of different current rates. The change of battery SOC is also plotted in Fig. 14.

The terminal voltage estimation result is shown in Fig. 15, with Fig. 16 revealing a closer look at the result in the interval 60–140 min. The MSE is calculated as $3.0542 \times 10^{-4}\,V^2$ with a maximum error voltage of 35.8 mV (mean error = 2.6 mV). The rated error is calculated as the maximum error voltage over the nominal voltage of the battery module as 0.0358 V/14.4 V = 0.25%,

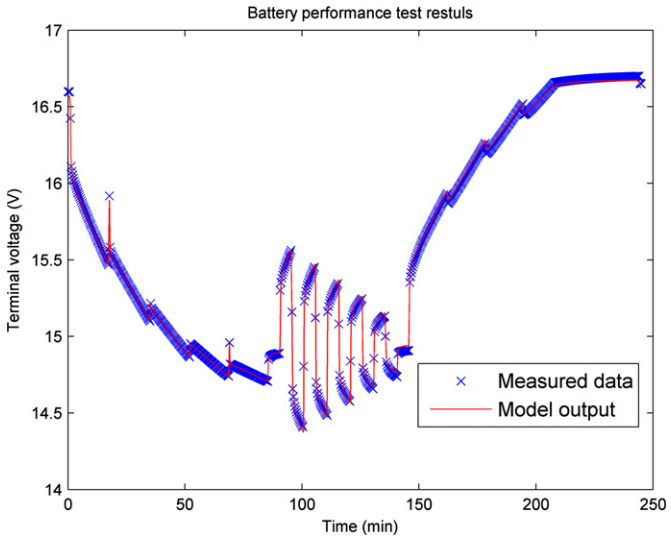

Fig. 15. Battery performance test result with a max rated error of 0.25%.

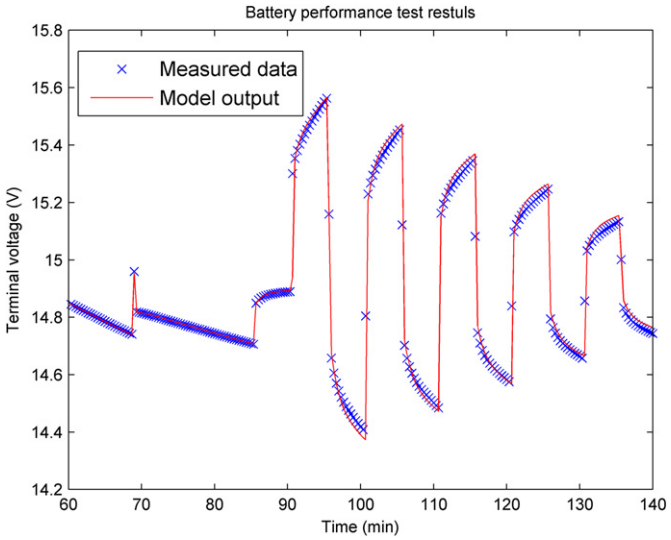

Fig. 16. Battery performance test results between 60–140 min.

which is even smaller than that usually experienced due to cell variation, which we believe is a result of cell averaging at the module level.

7. Conclusion

A bandwidth based electrical-analogue battery modeling procedure for battery modules is proposed in this paper. Battery behavior tests are designed to identify the battery parameters and extract the SOC–OCV profile. A detailed parameter identification and SOC–OCV profile extraction procedure is described based on a novel method for assigning time constants to the dynamic portion of this common modeling form. A 6.8 Ah Ultralife UBBL10 Li-ion battery module, which is considered a "microcosm" for a modern

large-format battery pack, was selected to verify the proposed procedure. Results show accurate voltage estimation with a max rated error of 0.25%. This paper is directed to module level battery modeling, which is the format of battery that is readily available in the marketplace. Such modules may have end use application themselves or they can be put together with multiple units to make larger battery systems. Since there is no battery chemistry specific characteristics involved in the reported work, this modeling procedure is clearly directly applicable to other battery chemistries such as the many forms of Li-ion, Nickel-Metal-Hydride and Lead-acid battery types.

References

[1] A. Khaligh, Z. Li, IEEE Transactions on Vehicular Technology 59 (2010) 2806–2814.
[2] C.C. Chan, Proceedings of the IEEE 90 (2002) 247–275.
[3] K. Smith, Chao-Yang Wang, Journal of Power Sources 160 (2006) 662–673.
[4] C.Y. Wang, V. Srinivasan, Journal of Power Sources 110 (2002) 364–376.
[5] M. Chen, G.A. Rincon-Mora, IEEE Transactions on Energy Conversion 21 (2006) 504–511.
[6] L. Gao, S. Liu, R.A. Dougal, IEEE Transactions on Components and Packaging Technologies 25 (2002) 495–505.
[7] R.C. Kroeze, P.T. Krein, in: Power Electronics Specialists Conference (2008) pp. 1336–1342.
[8] Y. Hu, S. Yurkovich, Y. Guezennec, B.J. Yurkovich, Control Engineering Practice 17 (2009) 1190–1201.
[9] O. Tremblay, L.-A. Dessaint, A.-I. Dekkiche, in: Vehicle Power and Propulsion Conference, IEEE, 2007, pp. 284–289.
[10] M. Pedram, IEEE Transactions on Very Large Scale Integration (VLSI) Systems 14 (2006) 441–451.
[11] J. Zhang, S. Ci, H. Sharif, M. Alahmad, in: Applied Power Electronics Conference and Exposition (APEC) (2010), pp. 672–675.
[12] J. Wang, K. Zou, C. Chen, L. Chen, in: Applied Power Electronics Conference and Exposition (APEC), IEEE, 2010, pp. 676–680.
[13] G. Plett, Journal of Power Sources 134 (2004) 262–276.
[14] A.A.H. Hussein, N. Kutkut, I. Batarseh, in: Applied Power Electronics Conference and Exposition (APEC) (2011) pp. 1790–1794.
[15] M. Dubarry, B.Y. Liaw, Journal of Power Sources 174 (2007) 856–860.
[16] Y. Hu, S. Yurkovich, Y. Guezennec, B.J. Yurkovich, Journal of Power Sources 196 (2011) 449–457.
[17] B. Schweighofer, K.M. Raab, G. Brasseur, IEEE Transactions on Instrumentation and Measurement 52 (2003) 1087–1091.
[18] K.M. Tsang, L. Sun, W.L. Chan, Energy Conversion and Management 51 (2010) 2857–2862.
[19] N.K. Medora, A. Kusko, in: Telecommunications Energy Conference (2006) pp. 1–8.
[20] S. Abu-Sharkh, D. Doerffel, Journal of Power Sources 130 (2004) 266–274.
[21] I.-S. Kim, Journal of Power Sources 163 (2006) 584–590.
[22] A. Vasebi, M. Partovibakhsh, S.M.T. Bathaee, Journal of Power Sources 174 (2007) 30–40.
[23] S. Pang, J. Farrell, J. Du, M. Barth, in: Proceedings of the American Control Conference (2001) pp. 1644–1649.
[24] M.S. Mazzola, N.H. Younan, R. Soundararajan, S.E. Saddow, Review of Scientific Instruments 69 (1998) 2459–2463.
[25] A.A. Istratov, O.F. Vyvenko, Review of Scientific Instruments 70 (1999) 1233–1257.
[26] G. Plett, Journal of Power Sources 161 (2006) 1369–1384.